

TUNNELING CURRENT NOISE SPECTRA OF BIASED IMPURITY WITH A PHONON MODE

N. S. Maslova^a, P. I. Arseev^b, V. N. Mantsevich^{a}*

^a Lomonosov Moscow State University
119991, Moscow, Russia

^b Lebedev Physical Institute, Russian Academy of Sciences
119991, Moscow, Russia

Received July 12, 2016

We report the results of theoretical investigations of the tunneling current noise spectra through a single-level impurity both in the presence and in the absence of electron–phonon interaction based on the nonequilibrium Green’s functions formalism. We show that due to the quantum nature of tunneling, the Fano factor is dramatically different from the Poisson limit both in the presence and in the absence of inelastic processes. The results are demonstrated to be sensitive to the tunneling contact parameters.

DOI: 10.7868/S0044451016110213

1. INTRODUCTION

Nanoscale tunneling junctions [1], formed by means of scanning tunneling microscopy (STM), provide broad possibilities for the analysis of electronic transport phenomena such as negative tunneling conductivity [2,3], suppression of shot noise [4,5], multiple charge redistribution, and inverse occupation formation [6,7] or phonons effects on the conductance and shot noise [8–10].

Nanoscale electronic devices demonstrate interesting equilibrium and nonequilibrium noise properties in a wide frequency range [11]. However, the main efforts were focused on the investigation of low-frequency shot noise [12–14], which is present in all kinds of devices and provides information on the electron transport mechanism [15–22].

Very often, counting statistics of photons produced by electronic shot noise is analyzed, but such an approximation ignores effects caused by the local density of states changing in the tunneling contact, which takes place due to the tunneling current flowing even in the absence of localized states formed by absorbed molecules, impurity atoms, or quantum dots. Electron tunneling processes through the individual molecule or

quantum dot localized in a tunneling junction excite its internal vibrational degrees of freedom. This effect strongly influences electron tunneling processes at low temperature, and consequently a large amount of experimental [23–26] and theoretical [27–30] work exists considering the problem of tunneling through a single level with strong coupling to the phonon mode. Unfortunately, most theoretical work concerning inelastic tunneling through an intermediate system is focused on the analysis of current characteristics. Only a few works were devoted to the shot noise problem [28–31] and tunneling current noise spectra were analyzed only in the zero-frequency case ($S(\omega = 0)$). Consequently, the problem of the tunneling current noise spectra analysis in nanoscale systems in the presence of electron–phonon interaction is still of great interest.

In this paper, we use the nonequilibrium Keldysh diagram technique to analyze tunneling current noise spectra for a single-level impurity both in the presence and in the absence of electron–phonon interaction in a wide frequency range. We demonstrate that due to the quantum nature of tunneling in nanoscale junctions, the Fano factor is strongly different from the Poisson limit both in the presence and in the absence of inelastic processes. We carefully analyze the tunneling current noise spectra in one of the contact leads $S(\omega)^{LL}$ in the presence of an impurity (absorbed molecule or quantum dot), which can be easily measured by the STM technique [13].

* E-mail: vmantsev@gmail.com

2. THE SUGGESTED MODEL AND MAIN RESULTS

2.1. Tunneling contact characteristics in the absence of localized states and electron–phonon interaction

We first consider the model of two tunneling contact leads and analyze the tunneling current characteristics in the absence of localized states and electron–phonon interaction. The Hamiltonian of this system involves two terms:

$$\hat{H} = \hat{H}_0 + \hat{H}_{tun}, \quad (1)$$

where \hat{H}_0 describes the two isolated leads:

$$\hat{H}_0 = \sum_{k \in L, \sigma} \varepsilon_k c_{k\sigma}^\dagger c_{k\sigma} + \sum_{p \in R, \sigma} (\varepsilon_p - eV) c_{p\sigma}^\dagger c_{p\sigma}. \quad (2)$$

Here, $c_{k(p)\sigma}^\dagger / c_{k(p)\sigma}$ are the creation/annihilation operators for the noninteracting electrons with momentum $k(p)$ and energy $\varepsilon_{k(p)}$ in the left L (sample) and right R (tip) lead of the tunneling contact.

The tunnel coupling between the leads is described by the Hamiltonian

$$\hat{H}_{tun} = \sum_{k, p, \sigma} T (c_{k\sigma}^\dagger c_{p\sigma} + c_{p\sigma}^\dagger c_{k\sigma}). \quad (3)$$

The tunneling amplitude T corresponds to the electron transfer between the tunneling contact leads and is assumed to be independent of the momentum and spin. We set $\hbar = 1$ and $e = 1$ in what follows. The tunneling current operator is

$$\hat{I} = \sum_{k \in L} \hat{n}_k = iT \sum_{k, p, \sigma} (c_{k\sigma}^\dagger(t) c_{p\sigma}(t) - c_{p\sigma}^\dagger(t) c_{k\sigma}(t)). \quad (4)$$

Our analysis deals with the low-temperature regime when the Fermi level is well defined and the temperature is much lower than all the typical energy scales in the system. Consequently, the distribution function of the electrons in the leads (band electrons) is close to the Fermi step. Without the Coulomb correlation, different spin channels are independent, and we can therefore omit the spin index σ . We consider the tunneling current and noise spectrum only for one spin channel, because the electron–phonon interaction does not mix spin degrees of freedom. An expression for the average tunneling current can be obtained with the use of nonequilibrium Keldysh Green's functions, which satisfy the system of equations

$$\begin{aligned} G_{kp}^< &= \sum_{p'} (G_{kk}^0 T G_{p'p})^<, \\ G_{kk'}^< &= G_{kk'}^0 \delta_{kk'} + \left(G_{kk}^0 T \sum_{p'} G_{p'k'} \right)^<. \end{aligned} \quad (5)$$

From these equations, one can find that

$$\begin{aligned} \sum_{k, k' \in L} G_{k,k'}^< &= \frac{2i\nu_L}{(1 + T^2 \nu_L \nu_R)^2} \times \\ &\times (n_k(\omega) + T^2 \nu_L \nu_R n_p(\omega)) = Z_{LL}^<(\omega), \end{aligned} \quad (6)$$

where ν_L and ν_R are unperturbed densities of states in the left and right leads of the tunneling contact and $n_{k(p)}(\omega)$ is the equilibrium electron distribution functions in the leads. This means that continuous-spectrum states in the right lead $n_p(\omega)$ contribute to the local nonequilibrium electron distribution in the left lead of the tunneling contact area. An expression for $Z_{RR}^<(\omega)$ can be obtained from (6) by changing the indices as $L \leftrightarrow R$:

$$\begin{aligned} \sum_{k, p} G_{pk}^< &= \frac{2T^2 \nu_L \nu_R}{(1 + T^2 \nu_L \nu_R)^2} \times \\ &\times (n_k(\omega) - n_p(\omega)) = Z_{LR}^<(\omega) \end{aligned} \quad (7)$$

and

$$\text{Im} \sum_{k, k' \in L} G_{k,k'}^A = \frac{\nu_L}{1 + T^2 \nu_L \nu_R} = \text{Im} Z_{LL}^A. \quad (8)$$

For a symmetric band, $\text{Re} Z_{LL}^A$ is equal to zero. Hence, the local density of states in the contact area is also modified by tunneling processes.

Finally, the expression for tunneling current has the form

$$I_{tun} = \int d\omega \frac{4T^2 \nu_L \nu_R}{(1 + T^2 \nu_L \nu_R)^2} [n_k(\omega) - n_p(\omega)]. \quad (9)$$

In the zero-temperature limit,

$$I_{tun} = \frac{4\eta}{(1 + \eta)^2} eV \quad (10)$$

with the parameter $\eta = T^2 \nu_L \nu_R$. The tunneling current noise spectrum is determined in terms of the tunneling current correlation function [10, 21, 22]

$$S^{\alpha\beta}(t, t') = \langle I_\alpha(t) I_\beta(t') \rangle, \quad (11)$$

where $\alpha, \beta = L, R$ and

$$S^{\alpha\beta}(\omega) = \int S^{\alpha\beta}(t, t') e^{i\omega(t-t')} d(t-t') \quad (12)$$

can be obtained from diagrams in Fig. 1a,b. By means of the Keldysh diagram technique, we can obtain the following expression for the tunneling current noise spectrum:

$$\begin{aligned} S(\omega) &= \int d\omega' [Z_{LL}^<(\omega + \omega') Z_{RR}^>(\omega') + \\ &+ Z_{LR}^<(\omega + \omega') Z_{RL}^>(\omega') + (L \leftrightarrow R)], \end{aligned} \quad (13)$$

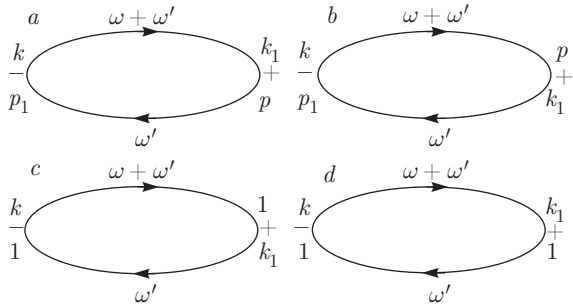


Fig. 1. Diagrams contributing to the tunneling current noise spectra without electron–phonon interaction: *a,b* in the case where tunneling processes occur between the tunneling contact leads and *c,d* in the case where tunneling processes occur through the localized state in the absence of electron–phonon interaction. One also has to consider diagrams with the indexes replaced as $k \leftrightarrow p$ for diagrams *a,b* and $k \leftrightarrow 1$ for diagrams *c,d*. Solid lines correspond to the Keldysh electron Green's functions in the presence of tunneling processes

where $Z_{\alpha\beta}^<(\omega)$ are given by Eqs. (6) and (7). To obtain expressions for $Z_{\alpha\beta}^>(\omega)$, we have to replace $n_{k(p)}(\omega)$ with $n_{k(p)}(\omega) - 1$. Straightforward calculations yield

$$S(\omega = 0; eV) = eV \left[\frac{8\eta(1 + \eta^2)}{(1 + \eta)^4} - \frac{8\eta^2}{(1 + \eta)^4} \right]. \quad (14)$$

We also analyzed the Fano factor, which measures the deviation from uncorrelated Poissonian noise. With expressions (10) and (14), the Fano factor is defined as:

$$F = \frac{S(\omega = 0; eV)}{2eI_{tun}} = \frac{1 + \eta^2 - \eta}{(1 + \eta)^2}. \quad (15)$$

Figure 2*a* demonstrates the Fano factor decreasing from $F = 1$ to $F = 1/4$ with an increase in the parameter η .

With the terms proportional to η^3 and higher omitted in the numerator in the zero-temperature limit, the tunneling current noise spectrum has the form

$$S(\omega) = \frac{8}{(1 + \eta)^4} [\eta(1 - \eta)[(\omega + eV)N(\omega + eV) + (\omega - eV)N(\omega - eV)] + 2\eta^2\omega N(\omega)], \quad (16)$$

where $N(\omega) = 1/(\exp(\omega/\vartheta) - 1)$ and ϑ is the temperature. For $\vartheta = 0$, the emission part of the noise spectrum ($eV > 0$ and $\omega > 0$) has the form

$$S(\omega) = \frac{8}{(1 + \eta)^4} \Theta(eV - \omega)\eta(1 - \eta)(eV - \omega). \quad (17)$$

A similar expression can be obtained from Eq. (16) for $\omega < 0$. The tunneling current noise spectrum is shown in Fig. 2*b* and demonstrates a linear decay

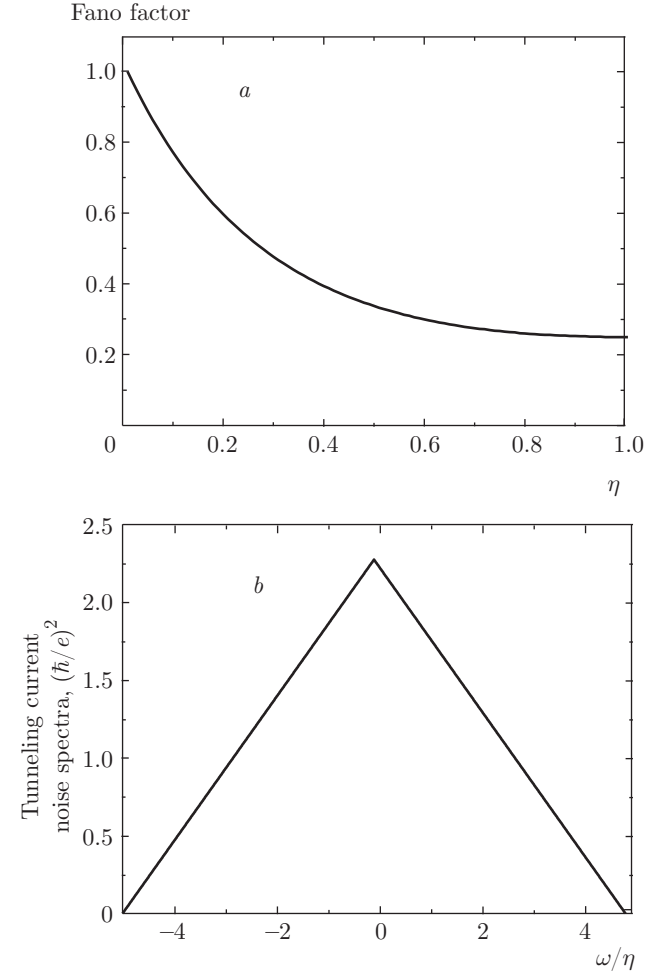


Fig. 2. *a*) Fano factor in the absence of impurities in the tunneling contact as a function of the parameter $\eta = T^2\nu_L\nu_R$. *b*) Tunneling current noise spectrum in the absence of impurities in the tunneling junction. $eV = 5$, $T = 1$, and $\nu_L = \nu_R = 1$

from the maximum value at $\omega = 0$ to zero at the frequency value equal to the applied bias eV . If we omit summation over the index p' in Eq. (5) and consider the contribution only from the diagonal Green's functions for the diagrams shown in Fig. 1, then the Landauer–Buttiker result is directly reproduced in the zero-frequency limit [32].

2.2. Tunneling contact characteristics in the presence of localized states and electron–phonon interaction

We now consider tunneling through a localized state with a single particle energy level ε both in the absence and in the presence of electron–phonon interaction, which is described by the Hamiltonian

$$\hat{H} = \hat{H}_0 + \hat{H}_{tun}, \quad (18)$$

where \hat{H}_0 describes isolated tunneling contact leads and a single-level intermediate impurity:

$$\hat{H}_0 = \varepsilon d^\dagger d + \sum_{k \in L, \sigma} \varepsilon_k c_k^\dagger c_k + \sum_{p \in L, \sigma} (\varepsilon_p - eV) c_p^\dagger c_p. \quad (19)$$

The indices k and p label continuous spectrum states in the respective left (sample) and right (tip) leads of the tunneling contact. The operators $c_{k(p)}^\dagger / c_{k(p)}$ correspond to electron creation/annihilation in the continuous spectrum states $k(p)$. The operator d^\dagger / d creates/destroys an electron on the spin-degenerate impurity energy level ε .

The tunneling Hamiltonian \hat{H}_{tun} in the presence of electron–phonon interaction in the general case contains two different constants g and λ and has the form [33]

$$\begin{aligned} \hat{H}_{tun} = & \sum_{k \in L} [T_k (c_k^\dagger d + d^\dagger c_k) + g T_k (b^\dagger + b) (c_k^\dagger d + d^\dagger c_k) + \\ & + \lambda T_k (b - b^\dagger) (c_k^\dagger d - d^\dagger c_k)] + (k \leftrightarrow p). \end{aligned} \quad (20)$$

The tunneling amplitudes T_k and T_p correspond to the tunneling processes between the impurity state and continuous spectrum states in the tunneling contact leads and are independent of the momentum $k(p)$. The operator b^\dagger / b corresponds to phonon creation/annihilation, ω_0 is the optical phonon frequency, and g is the electron–phonon coupling constant. The constant λ corresponds to an adiabatic change of the distance between atoms in the molecule, which change their position corresponding to the energy minimum for different electronic densities. The tunneling current operator for the lead $\alpha = L, R$ is given by

$$\begin{aligned} \hat{I}_\alpha(t) = & i \sum_{k \in \alpha} T_k \{ c_k^\dagger(t) d(t) + c_k^\dagger(t) d(t) \times \\ & \times [(g + \lambda) b(t) + (g - \lambda) b^\dagger(t)] - \text{H.c.} \}. \end{aligned} \quad (21)$$

In what follows, we consider the situation where $\lambda = 0$, because effects caused by the adiabatic distance changing between atoms in the molecule are not very important in the case where the total electron number in the molecule is not too small [33]. The current noise correlation function in the presence of a localized state is different for the left and right leads of tunneling contact. We consider the tunneling current noise correlation function for the left lead:

$$\begin{aligned} S^{LL}(t, t') = & \langle I_L(t) I_L(t') \rangle = \\ = & \sum_{k \in \alpha, k' \in \beta} T_k^2 \{ \{ c_k^\dagger(t) d(t) + g c_k^\dagger(t) d(t) b(t) + \\ & + g c_k^\dagger(t) d(t) b^\dagger(t) \} \{ d^\dagger(t') c_{k'}(t') + \\ & + g d^\dagger(t') c_{k'}(t') b^\dagger(t') + g d^\dagger(t') c_{k'}(t') b(t') \} \}. \end{aligned} \quad (22)$$

Using the Keldysh nonequilibrium Green's function formalism, we can obtain an expression for the tunneling current noise spectrum without the electron–phonon interaction by means of diagrams shown in Fig. 1c,d:

$$\begin{aligned} S_0^{LL}(\omega) = & \\ = & T_k^2 [Z_{LL}^{<T}(\omega + \omega') G_{11}^{>T}(\omega) + G_{11}^{<T}(\omega + \omega') Z_{LL}^{>T}(\omega)] + \\ & + T_k^2 \sum_{k, k_1 \in \alpha} [G_{k1}^{<T}(\omega + \omega') G_{k_1 1}^{>T}(\omega) + \\ & + G_{1k_1}^{<T}(\omega + \omega') G_{k_1 1}^{>T}(\omega)], \end{aligned} \quad (23)$$

where the Keldysh Green's functions are determined from the Dyson equations

$$\begin{aligned} G_{kk_1}^{<T} &= G_{kk}^{0<} \delta_{kk_1} + (G_{kk}^0 T_k G_{1k_1}^T)^<, \\ G_{k1}^{<T} &= G_{kk}^{0R} T_k G_{11}^{<T} + G_{kk}^{0<} T_k G_{11}^{AT}, \\ G_{11}^{<T} &= G_{11}^{0<} + \left(G_{11}^0 T_k \sum_k G_{k1}^T \right)^< \end{aligned} \quad (24)$$

and $Z_{LL}^{<T}(\omega)$ has the form

$$\begin{aligned} Z_{LL}^{<T}(\omega) = & \sum_{k, k' \in \alpha} G_{kk'}^{<T}(\omega) = \\ = & 2i\nu_L n_k(\omega) [1 - \gamma_{k1} \text{Im } G_{11}^{RT}(\omega)] + \\ + & 2i\nu_L \frac{\gamma_{k1}\gamma_{p1}}{\gamma_{k1} + \gamma_{p1}} \text{Im } G_{11}^{RT}(\omega) [n_p(\omega) - n_k(\omega)]. \end{aligned} \quad (25)$$

The expression for $Z_{LL}^{<T}(\omega)$ was obtained assuming that

$$G_{11}^< = -2i n_1(\omega) \text{Im } G_{11}^R(\omega), \quad (26)$$

where

$$n_1(\omega) = \frac{\gamma_{k1} n_k(\omega) + \gamma_{p1} n_p(\omega)}{\gamma_{k1} + \gamma_{p1}} \quad (27)$$

are nonequilibrium impurity filling numbers and

$$G_{11}^R = \frac{1}{\omega - \varepsilon + i(\gamma_{k1} + \gamma_{p1})} \quad (28)$$

is the impurity Green's function.

In our model, the relaxation rates γ_{ki} and γ_{pi} are determined by the electron tunneling transitions from

the impurity to the continuous spectrum states k and p in the respective left (L) and right (R) tunneling contact leads:

$$\sum_p T_p^2 \operatorname{Im} G_{pp}^{0R} = \gamma_{p1}; \quad \sum_k T_k^2 \operatorname{Im} G_{kk}^{0R} = \gamma_{k1}. \quad (29)$$

Depending on the tunneling barrier width and height, a typical tunneling coupling strength $\gamma_{k(p)i}$ can range from 10 μeV [34] to 1–5 meV [35]. We are interested in the situation where $\Gamma = \gamma_{p1} + \gamma_{k1}, kT \ll \ll |\varepsilon - E_F|, \omega_0$, and the applied bias voltage eV changes in a wide range. The opposite situation $\Gamma \gg eV, kT, \omega_0$ was considered in [36, 37]. An expression for the tunneling current noise spectrum without the electron–phonon interaction after substitution of the corresponding Green's functions can be written as

$$\begin{aligned} S_0^{LL}(\omega) = & 4\gamma_{k1} \int d\omega' \{ n_k(\omega + \omega') [n_1(\omega') - 1] \times \\ & \times [1 - \gamma_{k1} \operatorname{Im} G_{11}^R(\omega + \omega')] \operatorname{Im} G_{11}^R(\omega') + n_1(\omega + \omega') \times \\ & \times [n_k(\omega') - 1] [1 - \gamma_{k1} \operatorname{Im} G_{11}^R(\omega')] \operatorname{Im} G_{11}^R(\omega + \omega') \} + \\ & + \gamma_{k1} \int d\omega' \{ [n_1(\omega') - 1] I_T(\omega + \omega') \operatorname{Im} G_{11}^R(\omega') + \\ & + n_1(\omega + \omega') I_T(\omega') \operatorname{Im} G_{11}^R(\omega + \omega') \} - \\ & - 8\gamma_{k1}^2 \int d\omega' \operatorname{Im} G_{11}^R(\omega') \operatorname{Im} G_{11}^R(\omega + \omega') \times \\ & \times [n_1(\omega') - n_k(\omega')] [n_1(\omega + \omega') - n_k(\omega + \omega')], \quad (30) \end{aligned}$$

where

$$I_T(\omega) = \frac{4\gamma_{k1}\gamma_{p1}}{(\omega - \varepsilon)^2 + (\gamma_{k1} + \gamma_{p1})^2} [n_k(\omega) - n_p(\omega)]. \quad (31)$$

Expression (30) allows analyzing tunneling current noise spectra for the typical values of tunneling contact kinetic parameters in the absence of electron–phonon interaction in a wide frequency range. In Fig. 3, we plot the tunneling current noise spectra in the left tunneling contact lead related to the positive frequency part $\omega > 0$ as a function of the frequency and applied bias voltage eV . At $eV < \varepsilon$, tunneling current noise spectra (Fig. 3a solid lines) demonstrate very similar behavior for both symmetric $\gamma_k = \gamma_p$ and asymmetric $\gamma_k \neq \gamma_p$ tunneling contacts. Tunneling current noise spectra decay from the maximum value at $\omega = 0$ to zero at the frequency value equal to the applied bias eV (Fig. 3a, solid lines). At $eV > \varepsilon$, tunneling current noise spectra (Fig. 3a, dashed lines) exhibit a single peak around $\omega = eV - \varepsilon$, which is mostly pronounced for the symmetric tunneling contact and small relaxation rates. In the limit of large relaxation rates, for both $eV < \varepsilon$ and $eV > \varepsilon$ (Fig. 3b, solid and dashed lines), the tunneling current noise spectra reveal a shape very similar

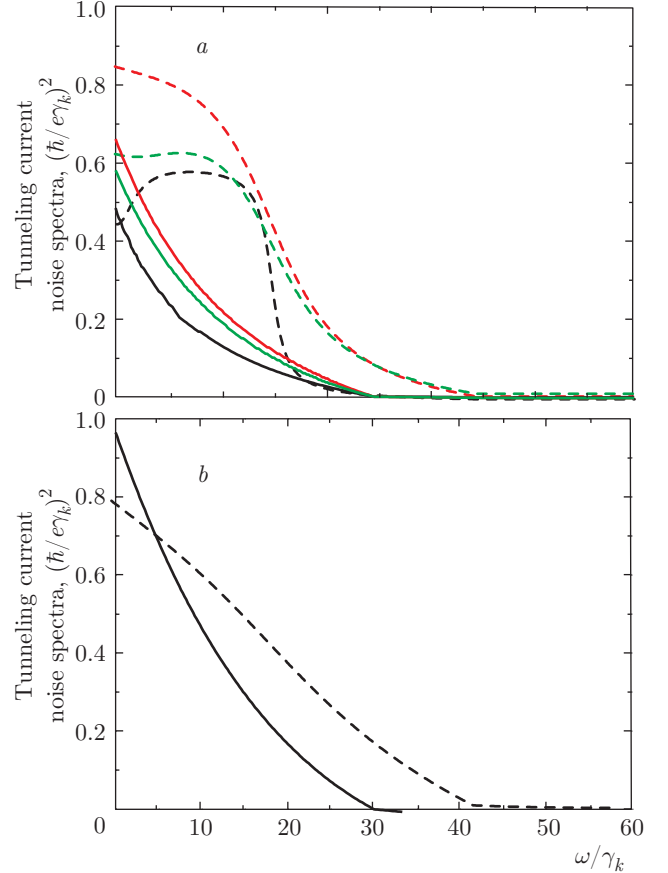


Fig. 3. (Color online) Tunneling current noise spectra in the left tunneling contact lead in the presence of an impurity state in the tunneling junction. Solid lines: $eV/\gamma_k = 30$; dashed lines: $eV/\gamma_k = 70$. a) $\gamma_k = 1, \gamma_p/\gamma_k = 1$: black lines (solid, dashed); $\gamma_k = 1, \gamma_p/\gamma_k = 10$: green lines (solid, dashed), $\gamma_k = 1, \gamma_p/\gamma_k = 0.1$: red lines (solid, dashed). b) $\varepsilon/\gamma_k = 2.6$, $\gamma_k = 1$, and $\gamma_p/\gamma_k = 1$

to the one obtained in the case where tunneling occurs directly between the tunneling contact leads (Fig. 2a).

Figure 4 shows the bias-dependent Fano factor for the system under investigation. In the low-bias-voltage region, below the single-level resonance $eV < \varepsilon$, the Fano factor is very close to $F = 1$. In contrast, in the high-bias-voltage regime ($eV > \varepsilon$), the Fano factor rapidly decreases and tends to $3/4$ for a symmetric noninteracting system $\gamma_k = \gamma_p$. The smallest Fano factor is observed at the resonance point $eV = \varepsilon$ for the symmetric tunneling contact, implying that the quantum nature of the tunneling processes significantly suppresses shot noise. The obtained results show that the Fano factor depends on the relaxation rates in both low- and high-bias-voltage regimes. Consequently, due to the quantum tunneling nature, even in the absence of electron–phonon interaction, the Fano factor differs

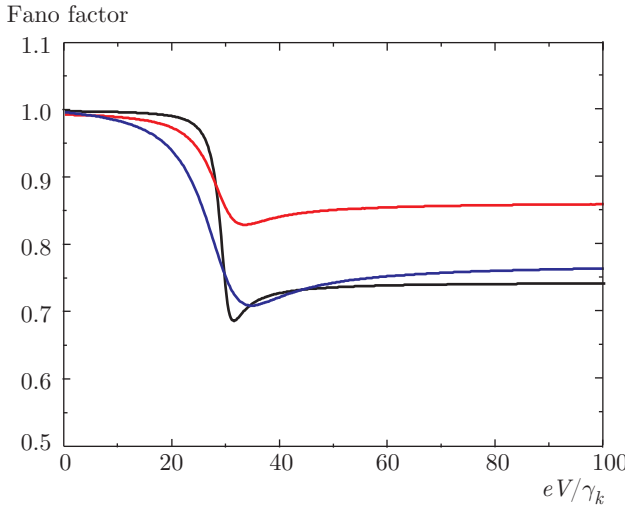


Fig. 4. (Color online) Fano factor as a function of the applied bias voltage in the case where tunneling processes occur through a localized state. Black line: $\varepsilon/\gamma_k = 30, \gamma_k = 1, \gamma_p/\gamma_k = 1$; red line: $\varepsilon/\gamma_k = 30, \gamma_k = 1, \gamma_p/\gamma_k = 4$; blue line: $\varepsilon/\gamma_k = 10, \gamma_k = 1, \gamma_p/\gamma_k = 1.3$

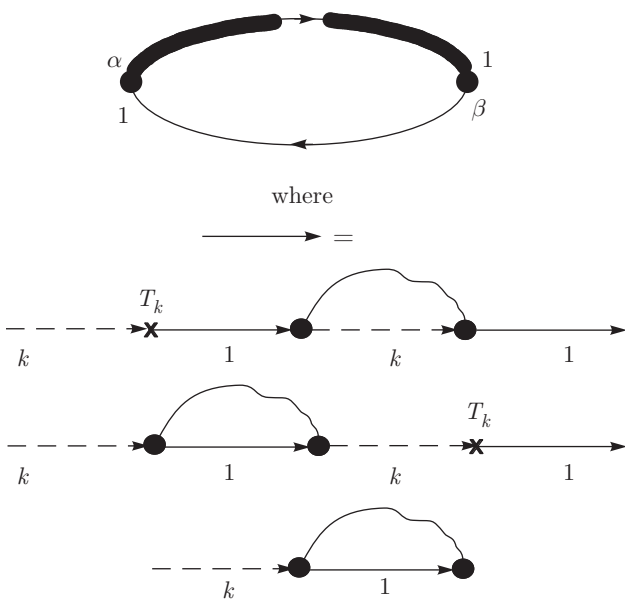


Fig. 5. Lowest-order diagrams contributing to the tunneling current noise spectrum $S_{11}^{LL}(\omega)$ in the presence of electron–phonon interaction. Dashed lines demonstrate the Green’s functions of unperturbed conduction electrons in the tunneling contact leads; solid lines correspond to the Keldysh electron Green’s functions in the presence of tunneling processes; wavy lines describe the phonon Green’s functions

from the Poisson limit, where electrons diffuse in an uncorrelated way.

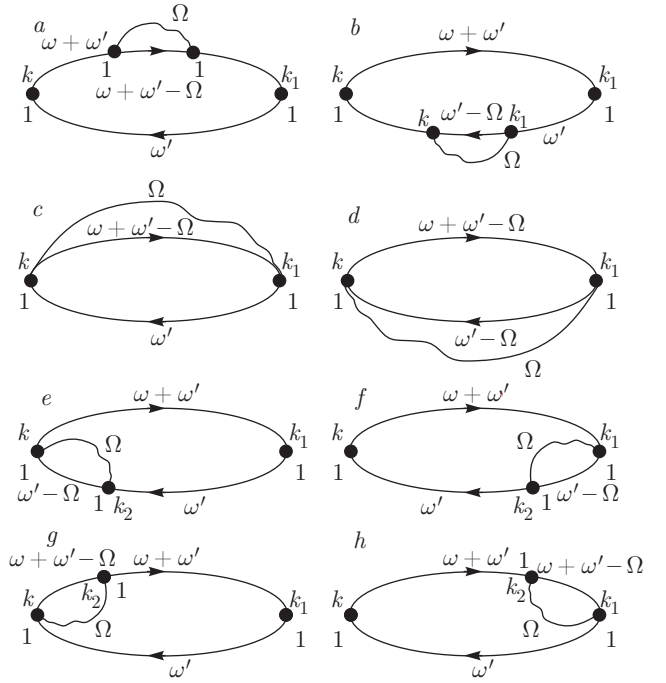


Fig. 6. Lowest-order diagrams contributing to the total tunneling current noise spectrum in the presence of electron–phonon interaction. One also has to consider diagrams with the indexes replaced as $k \leftrightarrow 1$. Diagrams a–d contribute to $S_{21}^{LL}(\omega)$. Diagrams e–h correspond to $S_{22}^{LL}(\omega)$, those with the indexes changed as $k \leftrightarrow 1$ correspond to $S_{23}^{LL}(\omega)$. Solid lines correspond to the Keldysh electron Green’s functions in the presence of tunneling processes; wavy lines describe the phonon Green’s functions

We now consider electron–phonon interaction, which gives new types of diagrams contributing to the tunneling current noise spectrum. These diagrams are shown in Figs. 5 and 6. In a perturbative treatment, nonvanishing terms start from g^2 ($g^2 \sim \sim 0.1$), if Bose-condensation processes are ignored. We mention that we neglect diagrams that involve vertex corrections, because they are of the order of $\max\{\Gamma/\omega_0, \Gamma/\varepsilon, \Gamma/(\varepsilon + \omega_0)\}$ compared with the leading contribution to the tunneling current noise spectrum from diagrams shown in Fig. 5.

The diagrams in Fig. 5 correspond to the following contribution to the tunneling current noise spectrum:

$$\begin{aligned} S_1^{LL}(\omega) = & \int d\omega' [I_T(\omega') I_T(\omega + \omega') + \\ & + (I^{el}(\omega + \omega') + I^{inel}(\omega + \omega')) I^T(\omega') + \\ & + (I^{el}(\omega') + I^{inel}(\omega')) I^T(\omega + \omega')]. \quad (32) \end{aligned}$$

The elastic part of the tunneling current is given by [33]

$$I^{el} = \int \left[4 \frac{\gamma_{k1}\gamma_{p1}}{\gamma_{k1} + \gamma_{p1}} \text{Im } G^{(1)R}(\omega) \right] \times \\ \times (n_p(\omega) - n_k(\omega)) \frac{d\omega}{2\pi}, \quad (33)$$

where

$$\text{Im } G_{11}^{(1)R}(\omega) = \text{Im} \left[G_0^{(1)R}(\omega) \Sigma^R(\omega) G_0^{(1)R}(\omega) \right] \quad (34)$$

and

$$G_0^{(1)R}(\omega) = \frac{1}{\omega - \varepsilon - i(\gamma_k + \gamma_p)}.$$

The self-energy part Σ^R is given by the interaction with phonons:

$$\Sigma^R(\omega) = iT_k^2 \int \sum_k [\tilde{D}_k^R(\Omega) G_k^<(\omega - \Omega) + \\ + \tilde{D}_k^>(\Omega) G_k^R(\omega - \Omega)] d\Omega + iT_p^2 \int \sum_p [\tilde{D}_p^R(\Omega) G_p^<(\omega - \Omega) + \\ + \tilde{D}_p^>(\Omega) G_p^R(\omega - \Omega)] d\Omega, \quad (35)$$

where

$$\begin{aligned} \tilde{D}_{k(p)}^R(\Omega) &= g^2 D^R(\Omega) + g^2 D^A(-\Omega), \\ \tilde{D}_{k(p)}^<(\Omega) &= g^2 D^<(\Omega) + g^2 D^>(-\Omega), \\ \tilde{D}^<(\Omega) &= 2iN(\Omega) \text{Im } \tilde{D}^R(\Omega). \end{aligned} \quad (36)$$

Here, $N(\Omega)$ is the phonon distribution function, which in the general case is nonequilibrium and can be found self-consistently, taking the excitation of vibrational modes by the tunneling current into account [33], and

$$D^R(\omega) = \frac{1}{\Omega - \omega_0 + i\delta}. \quad (37)$$

The inelastic part of the tunneling current is [33]

$$\begin{aligned} I^{inel} = \int 4 \frac{\gamma_{k1}\gamma_{p1}}{(\gamma_{k1} + \gamma_{p1})^2} \text{Im } G^{(1)A}(\omega) \frac{d\omega}{2\pi} \times \\ \times \int \frac{d\Omega}{2\pi} (n_k(\omega) - n_p(\omega)) \times \\ \times [\gamma_{k1} \text{Im } \tilde{D}_p^A \{1 + N(\Omega) - n_p(\omega - \Omega)\} + \\ + \gamma_{p1} \text{Im } \tilde{D}_k^A \{1 + N(\Omega) - n_k(\omega - \Omega)\}]. \end{aligned} \quad (38)$$

The contribution to the tunneling current noise spectrum from the diagrams in Fig. 6 is given by

$$S_2^{LL}(\omega) = S_{21}^{LL}(\omega) + S_{22}^{LL}(\omega) + S_{23}^{LL}(\omega), \quad (39)$$

where

$$\begin{aligned} S_{21}^{LL}(\omega) = T_k^2 g^2 [Z_{LL}^{<T}(\omega + \omega' - \Omega) D^<(\Omega) G_{11}^{>T}(\omega') + \\ + G_{11}^{<T}(\omega + \omega' - \Omega) D^<(\Omega) Z_{LL}^{>T}(\omega')] + \\ + T_k^2 g^2 [Z_{LL}^{<T}(\omega + \omega') G_{11}^{>(1)}(\omega') + \\ + G_{11}^{<(1)}(\omega + \omega') Z_{LL}^{>T}(\omega')] + \\ + T_k^2 g^2 [Z_{LL}^{<(1)}(\omega + \omega') G_{11}^{>T}(\omega') + \\ + G_{11}^{<T}(\omega + \omega') Z_{LL}^{>(1)}(\omega')], \end{aligned} \quad (40)$$

$$\begin{aligned} S_{22}^{LL}(\omega) = g^2 G_{11}^{>T}(\omega') \{ I_T(\omega + \omega') \times \\ \times [\Sigma_{11}^A(\omega + \omega') - \Sigma_{11}^R(\omega + \omega')] + \\ + \Sigma_{11}^<(\omega + \omega') i\gamma_{k1} [G_{11}^{AT}(\omega + \omega') - \\ - G_{11}^{RT}(\omega + \omega')] \} + g^2 Z_{LL}^{<T}(\omega + \omega') \{ I_T(\omega') \times \\ \times [\Sigma_{LL}^R(\omega') - \Sigma_{LL}^A(\omega')] + \\ + \Sigma_{LL}^>(\omega') i\gamma_{k1} [G_{11}^{AT}(\omega') - G_{11}^{RT}(\omega')] \}, \end{aligned} \quad (41)$$

and

$$\begin{aligned} S_{23}^{LL}(\omega) = g^2 Z_{LL}^{>T}(\omega') \{ I_T(\omega + \omega') \times \\ \times [\Sigma_{LL}^R(\omega + \omega') - \Sigma_{LL}^A(\omega + \omega')] + \\ + \Sigma_{LL}^<(\omega + \omega') i\gamma_{k1} [G_{11}^{AT}(\omega + \omega') - \\ - G_{11}^{RT}(\omega + \omega')] \} + g^2 G_{11}^{<T}(\omega + \omega') \times \\ \times \{ I_T(\omega') [\Sigma_{11}^A(\omega') - \Sigma_{11}^R(\omega')] + \\ + \Sigma_{11}^>(\omega') i\gamma_{k1} [G_{11}^A(\omega') - G_{11}^{RT}(\omega')] \} \end{aligned} \quad (42)$$

with

$$\begin{aligned} Z_{LL}^{<(1)}(\omega) = \sum_{kk'\epsilon\alpha} G_{kk'}^{<(1)}(\omega) = 2T_k^2 \nu_\alpha^2 g^2 N(\omega_0) \times \\ \times G_{11}^{<T}(\omega - \omega_0) + 2\nu_\alpha^2 g^2 n_k(\omega) (\Sigma_{LL}^A(\omega) - \Sigma_{LL}^R(\omega)) \end{aligned} \quad (43)$$

and the self-energy parts of the form

$$\begin{aligned} \Sigma_{11}^<(\omega) &= 2iN(\omega_0) T_k^2 Z_{LL}^{<T}(\omega - \omega_0), \\ \Sigma_{LL}^<(\omega) &= -4iN(\omega_0) T_k^2 n_1(\omega - \omega_0) \times \\ &\times \text{Im } G_{11}^{RT}(\omega - \omega_0), \end{aligned} \quad (44)$$

$$\Sigma_{11}^A(\omega) - \Sigma_{11}^R(\omega) = 2i\gamma_k(N(\omega_0) + 1 - n_k(\omega - \omega_0)), \quad (45)$$

$$\begin{aligned} \Sigma_{LL}^R(\omega) - \Sigma_{LL}^A(\omega) = 2iT_k^2 [n_d(\omega - \omega_0) - N(\omega_0) - 1] \times \\ \times \text{Im } G_{11}^{RT}(\omega - \omega_0), \end{aligned} \quad (46)$$

and

$$\begin{aligned} G_{11}^{<(1)}(\omega) = 2in_1(\omega) \text{Im } G_{11}^{(1)R}(\omega) + n_1(\omega) G_{11}^{RT}(\omega) \times \\ \times [\Sigma_{11}^R(\omega) - \Sigma_{11}^A(\omega)] G_{11}^{AT}(\omega) - \\ - G_{11}^{RT}(\omega) \Sigma_{11}^<(\omega) G_{11}^{AT}(\omega). \end{aligned} \quad (47)$$

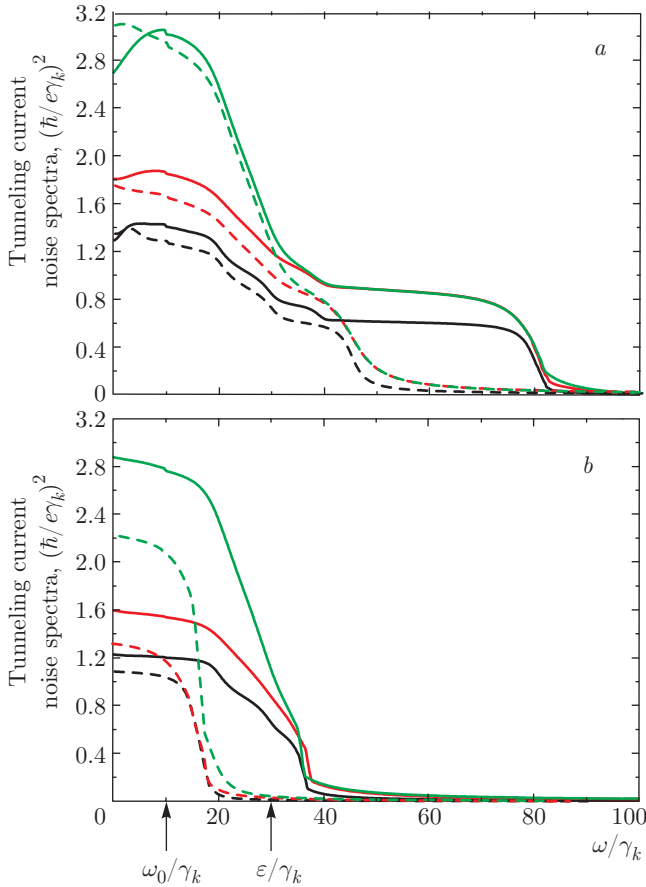


Fig. 7. (Color online) Tunneling current noise spectra in the left tunneling contact lead in the presence of electron–phonon interaction as a function of frequency. $\gamma_k = 1$, $\gamma_p/\gamma_k = 1$: black lines; $\gamma_k = 1$, $\gamma_p/\gamma_k = 3$: red lines; $\gamma_k = 1$, $\gamma_p/\gamma_k = 0.3$: blue lines. The parameters $\varepsilon/\gamma_k = 30$, $\omega_0/\gamma_k = 10$, and $g/\gamma_k = 7$ are the same for all figures. a) $eV/\gamma_k = 70$: solid lines, $eV/\gamma_k = 35$: dashed lines; b) $eV/\gamma_k = 26$: solid lines, $eV/\gamma_k = 6$: dashed lines

Figure 7 shows the tunneling current noise spectra in the left tunneling contact lead. We plot the results for both symmetric and asymmetric tunneling contacts and analyze four different areas of the bias voltage range: $eV < \omega_0$, $\omega_0 < eV < \varepsilon$, $\varepsilon < eV < \varepsilon + \omega_0$, and $\varepsilon + \omega_0 < eV$. First of all, we note that the edge of the tunneling current noise spectra in the presence of electron–phonon interaction is displaced by the value of the phonon frequency ω_0 in comparison with the case where the electron–phonon interaction is neglected, and consequently the spectra are cut off at $\omega = eV + \omega_0$. When the applied bias exceeds the typical phonon frequency ω_0 and the localized state energy level value ε , additional peculiarities arise in the tunneling current noise spectra (Fig. 7). These peculiarities are well

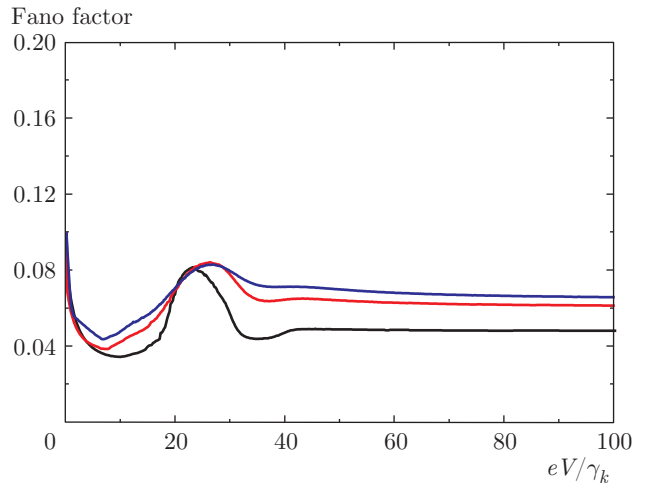


Fig. 8. (Color online) Additional contribution to the Fano factor caused by the presence of electron–phonon interaction as a function of the applied bias voltage in the presence of an impurity in the tunneling junction. Black line: $\varepsilon/\gamma_k = 30$, $\gamma_k = 1$, $\gamma_p/\gamma_k = 1$; red line: $\varepsilon/\gamma_k = 30$, $\gamma_k = 1$, $\gamma_p/\gamma_k = 4$; blue line: $\varepsilon/\gamma_k = 10$, $\gamma_k = 1$, $\gamma_p/\gamma_k = 1.3$. The parameters $\omega_0/\gamma_k = 10$ and $g/\gamma_k = 7$ are the same for all figures

pronounced around $\omega \simeq \omega_0$, $\omega \simeq \varepsilon$, and $\omega \simeq \varepsilon + \omega_0$. Depending on the segment of the bias voltage range, we can observe all three peculiarities (Fig. 7a), two of them ($\omega \simeq \omega_0$ and $\omega \simeq \varepsilon$) (Fig. 7b, solid lines), or only one ($\omega \simeq \omega_0$) (Fig. 7b, dashed lines).

An additional contribution to the Fano factor caused by the presence of electron–phonon interaction is shown in Fig. 8. This contribution slightly enhances the system Fano factor and exhibits a finer structure due to the presence of electron–phonon interaction. The existence of several dips in the Fano factor indicates the enhancement of the tunneling current at $eV \simeq \omega_0$, $eV \simeq \varepsilon$ and $eV \simeq \omega_0 + \varepsilon$. The obtained results demonstrate that the Fano factor is sensitive to the interaction with phonons.

3. CONCLUSION

We theoretically analyzed the tunneling current noise spectra both in the presence and in the absence of a localized state in the tunneling contact area in a wide frequency range based on the Keldysh Green's function formalism.

We found that even in the absence of a localized state, the tunneling current noise and the Fano factor are both influenced by changes in the local density of states and the nonequilibrium electron distribution in the contact area. We revealed that due to the quantum

nature of tunneling in nanoscale junctions, the Fano factor is strongly different from the Poisson limit both in the presence and in the absence of inelastic processes. The frequency-dependent tunneling current noise spectrum in the presence of an impurity state is strongly influenced by the applied bias voltage and the values of tunneling rates. The shape of the tunneling current noise spectrum considerably changes when the value of applied bias exceeds the impurity state energy for small tunneling rates. When the tunneling rates are of the order of the impurity state energy, additional peculiarities in the tunneling current noise spectrum are smoothed. In the presence of electron–phonon interaction, the edge of the tunneling current noise spectrum is shifted to the high-frequency region. The shift value is determined by the phonon frequency. Moreover, in the presence of electron–phonon interaction, some new peculiarities in the tunneling current noise spectrum determined by the phonon frequency are observed.

This work was supported by the Russian Federation President Grant for Young Scientists MD-4550-2016.2 and by RFBR grants.

REFERENCES

1. N. Agrait, A. Levy Yeyati, and J. M. van Ruitenbeek, Phys. Rep. **377**, 81 (2003).
2. P. I. Arseyev, N. S. Maslova, and V. N. Mantsevich, Europ. Phys. J. B **85**(12), 410 (2012).
3. P. I. Arseyev, N. S. Maslova, and V. N. Mantsevich, JETP **115**, 141 (2012).
4. H. E. van den Brom and J. M. van Ruitenbeck, Phys. Rev. Lett. **82**, 1526 (1999).
5. N. L. Schneider, G. Schull, and R. Berndt, Phys. Rev. Lett. **105**, 026601 (2010).
6. P. I. Arseyev, N. S. Maslova, and V. N. Mantsevich, JETP Lett. **94**, 390 (2011).
7. I. S. Beloborodov, A. V. Lopatin, V. M. Vinokur, and K. B. Efetov, Rev. Mod. Phys. **79**, 469 (2007).
8. N. Agrait, C. Untiedt, G. Rubio-Bollinger, and S. Vierra, Phys. Rev. Lett. **88**, 216803 (2002).
9. M. Kumar, R. Avriller, A. L. Yeyati, and J. M. van Ruitenbeek, Phys. Rev. Lett. **108**, 146602 (2012).
10. K. Kaasbjerg and A. Nitzan, Phys. Rev. Lett. **114**, 126803 (2015).
11. Sh. Kogan, *Electronic Noise and Fluctuations in Solids*, Cambridge Univ. Press, Cambridge (1996).
12. M. J. M. de Jong and C. W. J. Beenakker, *Mesoscopic Electron Transport*, Kluwer, Netherlands (1997).
13. A. I. Oreshkin, V. N. Mantsevich, N. S. Maslova, D. A. Muzychko, S. I. Oreshkin, V. I. Panov, S. V. Savinov, and P. I. Arseyev, JETP Lett. **85**, 40 (2007).
14. V. N. Mantsevich, N. S. Maslova, and G. Cao, JETP **121**, 259 (2015).
15. G. B. Lesovik, Sov. Phys. JETP Lett. **49**, 592 (1989).
16. M. Buttiker, Sov. Phys. Rev. Lett. **65**, 2901 (1990).
17. C. W. J. Beenakker and H. van Houten, Phys. Rev. B **43**, 12066 (1991).
18. Th. Martin and R. Landauer, Phys. Rev. B **45**, 1742 (1992).
19. A. H. Steinbach, J. M. Martinis, and M. H. Devoret, Phys. Rev. Lett. **76**, 3806 (1996).
20. Ya. M. Blanter and M. Buttiker, Phys. Rep. **336**, 1 (2000).
21. V. N. Mantsevich and N. S. Maslova, Sol. State Comm. **147**, 278 (2008).
22. V. N. Mantsevich and N. S. Maslova, JETP Lett. **89**, 24 (2009).
23. J. Chen, M. Reed, A. Rawlett, and J. Tour, Science **286**, 1550 (1999).
24. W. Liang, M. P. Shores, M. Brockrath, J. R. Long, and H. Park, Nature **417**, 725 (2002).
25. H. Park, J. Park, A. Lim, E. Anderson, A. Alvisatos, and P. McEuen, Nature **407**, 57 (2000).
26. H. Lam and D. Natelson, Nano Lett. **4**, 79 (2004).
27. U. Lundin and R. H. McKenzie, Phys. Rev. B **66**, 075303 (2002).
28. J.-X. Zhu and A. V. Balatsky, Phys. Rev. B **67**, 165326 (2003).
29. A. Mitra, I. Aleiner, and A. J. Millis, Phys. Rev. B **69**, 245302 (2004).
30. B. Dong, H. L. Cui, X. L. Lei, and N. J. M. Horing, Phys. Rev. B **71**, 045331 (2005).
31. R. Aguado and T. Brandes, Phys. Rev. Lett. **92**, 206601 (2004).

32. M. Buttiker, Y. Imri, R. Landauer, and S. Pinhas, Phys. Rev. B **31**, 6207 (1985).
33. P. I. Arseev and N. S. Maslova, Physics–Uspekhi **53**, 1151 (2010).
34. S. Haupt, W. Izumida, T. Hatano, S. Teraoka, S. Tarucha, J. A. Gupta, and D. G. Austing, Phys. Rev. Lett. **110**, 016803 (2013).
35. J. Fransson, Phys. Rev. B **69**, 201304 (2004).
36. F. Haupt, T. Novotny, and W. Belzig, Phys. Rev. Lett. **103**, 136601 (2009).
37. F. Haupt, T. Novotny, and W. Belzig, Phys. Rev. B **82**, 165441 (2010).